

Strong-Weak Bi-Adjoints, Gluon-W Resonances, and New Asymmetric LHC Production Processes

Linda M. Carpenter^{1,*} and Katherine Schwind^{1,†}

¹*Department of Physics, The Ohio State University and Center for Cosmology and AstroParticle Physics
191 W. Woodruff Ave, Columbus OH, 43201 U.S.A.*

We study a novel production and decay mechanism for a bi-adjoint spin zero particle in the $(8, 3, 0)$ representation of the Standard Model gauge groups. This work is part of a series studying new production processes for exotic particles in higher representations of Standard Model color and weak charge. Here, we study a specific new dimension 5 effective operator model which couples an exotic bi-adjoint scalar field to the $SU(3)$ and $SU(2)$ field strength tensors. The W-gluon resonant decay of the charged component of this new exotic field is explored. We discuss LHC production modes of both the charged and neutral bi-adjoint states and find a new single production mode for the charged state. This is the dominant LHC production mode for TeV-scale masses. We introduce a new HL-LHC search in which a single bi-adjoint is produced in association with a hard forward quark jet from asymmetric W-gluon fusion. This search yields a 5-sigma discovery potential for bi-adjoint masses up to 3 TeV for 10 TeV scalar effective operator cutoffs. We also find 2-sigma sensitivity at the HL-LHC for bi-adjoint masses up to 4 TeV and effective cutoffs in the 15 TeV range for the full 3 inverse atto-barn data set.

I. INTRODUCTION

This work is part of a series exploring new Light Exotic (LEX) particles that couple to the Standard Model through effective operators. In this series, we catalog under-explored and uncharted phenomenology for exotic particles with unusual Standard Model (SM) charges [1–6]. Since we do not know what new physics the universe might have in store for us, general EFT model-building techniques allow us to survey a broad landscape of potential new interactions. Models with exotic states that carry both large $SU(3)$ and $SU(2)$ charges are among those with the most compelling and still understudied phenomenology. Studies of BSM scenarios with exotic particles charged under $SU(3)$ tend to assume that the exotic particles are singlets under $SU(2)$. Some of the most well-known exotics models of this type include neutral color octet scalars, neutral fermionic color octets like gluinos, and $SU(2)$ singlet color sextets [2–4, 7–9]. Colored particles with $SU(2)$ representations that are fundamental and higher have received less attention with the noted exception of left-handed squarks and Manohar-Wise weak doublet color octets [10]. Both of these last examples are $SU(2)$ doublets, the lowest non-trivial representation of $SU(2)$.

In this work, we propose studying exotics in higher-dimensional representations of $SU(3)$ and $SU(2)$ which might have unusual effective couplings to Standard Model fields. Specifically, we study a scalar field in the adjoint representations of both the $SU(3)$ and $SU(2)$ gauge groups. The field we study has zero hypercharge, and we thus denote this "bi-adjoint" as being in the $(8, 3, 0)$ representation of the SM gauge groups.

Studies of exotic color octets have been quite limited. Many phenomenological studies have been conducted on neutral color octets in the $(8, 1, 0)$ representation of SM gauge groups [9, 11–16]. Less phenomenological attention has fallen on the aforementioned Manohar-Wise model, involving an $SU(2)$ doublet color octet in the $(8, 2, 1)$ representation of the SM, but several efforts have still been made to explore its phenomenological parameter space [17–19]. The Manohar-Wise field may couple directly to pairs of quarks at tree level. Both the $(8, 1, 0)$ and $(8, 2, 1)$ exotic octets have the feature that their neutral components can be singly produced through gluon fusion. This is a primary feature of their collider phenomenology, and di-jet resonances are an important discovery signature for them.

Conversely, the $(8, 3, 0)$ bi-adjoint is interesting because it has no renormalizable couplings to quarks. Furthermore, bi-adjoint single production through gluon fusion occurs only at dimension 7 in effective field theory, through an operator suppressed by a scale v^2/Λ^3 . Since the di-gluon and di-quark couplings of the bi-adjoint are suppressed, the main phenomenological signatures of the bi-adjoint model are significantly different and varied from previously explored color octet models.

Effective operators at dimension 5 are important to many color octet models. Indeed, it is a dimension 5 operator that generates the coupling to two gluons, allowing single production of color octets through gluon fusion in the $(8, 1, 0)$ and $(8, 2, 1)$ models. The bi-adjoint couples to the Standard Model through the dimension 5 effective operator

$$\frac{1}{\Lambda} \phi W^{\mu\nu} G_{\mu\nu} , \quad (1)$$

where ϕ is the bi-adjoint scalar. This operator was first discussed in references [1], [6], and [5], which cataloged new types of exotic states that could be reached through the W-gluon portal. The W-gluon portal is an unusual sector of the di-boson portal, the region of theory space where exotic particles couple to the SM through pairs of SM gauge bosons.

This new operator allows a host of new and unusual collider production modes for the bi-adjoint. The interactions it describes contain interesting couplings between the charged component of ϕ and a pair of W-gluon gauge bosons. This allows a new W-gluon resonant decay mode of the charged components of the bi-adjoint. The neutral component can similarly have Z-gluon/Z-photon decays. In this work, we explore the mass spectrum of the bi-adjoint model and the unusual di-boson couplings of the bi-adjoint states. We also discuss new single production modes for the charged and neutral bi-adjoints that result from the dimension 5 operator, focusing on production modes that follow from the W-gluon coupling. We introduce a new asymmetric LHC production mode for ϕ single production that involves an asymmetric W-gluon fusion process where a gluon fuses with a W boson that radiates off of an incoming quark. A single LEX state ϕ is then produced in association with a hard forward jet. We create a new HL-LHC sensitivity analysis and find that we have a 5σ discovery potential for ϕ masses in the multi-TeV range for cutoffs over 10 TeV. We also have a 2σ sensitivity to multi-TeV scalars with cutoffs up to 20 TeV.

This paper proceeds as follows. In Section 2 we introduce the model. In Section 3 we discuss decays of the bi-adjoints. In Section 4 we discuss LHC production modes. In Section 5 we propose a new search for charged bi-adjoints and perform an HL-LHC sensitivity analysis. Section 6 concludes.

II. MODEL

With this model, we consider the couplings of a spin-0 scalar in the $(8, 3, 0)$ representations of the $SU(3)$, $SU(2)$, and $U(1)$ gauge groups. We refer to this state as the "bi-adjoint" as it is in the adjoint representations of both the $SU(3)$ and $SU(2)$ gauge groups. This is thus a model of an exotic color octet with higher $SU(2)$ charge. We start by exploring the Lagrangian.

First, note that the bi-adjoint has components with electric charge $+1, 0, -1$. The $SU(2)$ adjoint may be expressed in the real representation, written in 2×2 matrix form as

$$\phi = \begin{pmatrix} \phi_0/\sqrt{2} & \phi^+ \\ \phi^- & -\phi^0/\sqrt{2} \end{pmatrix}. \quad (2)$$

This new field has standard kinetic terms. Writing this with the most general tree-level mass terms and dimension 4 Higgs interaction terms, we have

$$L_{0R} = |D_\mu \phi|^2 + M^2 Tr[\phi\phi] + y|H_k|^2 Tr(\phi\phi) + \delta\phi^3 + quartics. \quad (3)$$

In the above Lagrangian, ϕ is the $(8, 3, 0)$ bi-adjoint field and H is the Standard Model Higgs field. Lowercase letters indicate $SU(2)$ fundamental indices. The parameter M is a standard mass shared by all of the components of ϕ . For this real representation, there is only one independent Higgs coupling term. Both this term and the mass term couple to $Tr[\phi\phi]$. In the real representation, the masses of the charged and neutral states are not split by the Higgs interaction, and all states in the multiplet are degenerate. There is an allowed trilinear coupling of the bi-adjoint proportional to a parameter δ , which has dimensions of mass. The quartic terms involving the bi-adjoints are enumerated in the appendix.

Instead, we can let ϕ be a complex field, with real and imaginary components $\phi = \phi_R + i\phi_I$. Counting the real and imaginary states of different charges, there are six total components of ϕ . This Lagrangian is considerably more complicated than the real model.

$$L_{0C} = |D_\mu \phi|^2 + m^2 \phi\phi^\dagger + \frac{1}{2}M^2 Tr[\phi\phi] + \frac{1}{2}\lambda_1|H_k|^2 Tr(\phi\phi) + \lambda_2|H_k|^2 \phi\phi^\dagger + \lambda_3(H^{\dagger k}\phi_j^j)(\phi_j^{i\dagger}H_i) + \lambda_4(H^{\dagger k}\phi_k^j)(\phi_j^iH_i) + \lambda_5(H^{\dagger k}\phi_k^j)(\phi_j^iH_i) + \delta\phi^3 + \delta_2\phi|\phi|^2 + quartics + h.c. \quad (4)$$

The Lagrangian in Eq. 4 is similar to the Lagrangian for a Higgs triplet field [20–23] and to the scalar potential of supersymmetric theories with pure $SU(2)$ adjoints [24–26]. However, it differs in some key features such that we have to take care with CP conservation. For complex bi-adjoint fields, there is a possible mass term m^2 involving $\phi\phi^\dagger$ and a second type of mass term M^2 involving $\phi\phi$ plus its hermitian conjugate. This latter type of mass is not allowed in triplet Higgs models due to hypercharge conservation. In this model, the mass parameter M splits the masses of

the real and imaginary components of ϕ . Furthermore, there are several new possible Higgs interactions allowed by all symmetries. The parameter λ_1 further splits the masses of the real and imaginary states. When Higgs vevs are inserted, λ_2 provides a mass term similar to m^2 . However, after the insertion of Higgs vevs, the λ_3 and λ_4 terms split the masses between the differently charged states. This splitting has an analog from a similar operator in the Higgs triplet model. The neutral mass eigenstates are

$$m_{\phi_R^0}^2 = (m^2 + (\lambda_1 + \lambda_2)v^2 + M^2 + \lambda_5v^2 + \lambda_3\frac{v^2}{2} + \lambda_4\frac{v^2}{2}) , \quad (5)$$

$$m_{\phi_I^0}^2 = (m^2 + (-\lambda_1 + \lambda_2)v^2 - M^2 - \lambda_5v^2 + \lambda_3\frac{v^2}{2} + \lambda_4\frac{v^2}{2}) . \quad (6)$$

To compute the masses of charged states we must diagonalize the mass matrix

$$\begin{matrix} \phi^+ & & \phi^{-\dagger} \\ \phi^{+\dagger} & \begin{pmatrix} m^2 + \lambda_2v^2 + \lambda_3v^2 & M^2 + \lambda_1v^2 + \lambda_5v^2 \\ M^2 + \lambda_1v^2 + \lambda_5v^2 & m^2 + \lambda_2v^2 + \lambda_4v^2 \end{pmatrix} \\ \phi^- & & \end{matrix} .$$

For the mass eigenstates of the charged states to be pure real or imaginary ϕ components, the off diagonal parameters M and $\lambda_{1,5}$ must be zero if $\lambda_3 \neq \lambda_4$.

The kinetic term contains couplings of the ϕ components to SU(2) and SU(3) gauge bosons. Particularly important is the interaction which couples the charged and neutral components of the ϕ field to a W boson as shown in Fig. 1. If the mass splitting parameter is non-zero, these interactions allow either the charged or neutral component of ϕ to decay to an on- or off-shell W boson and the lighter bi-adjoint component.

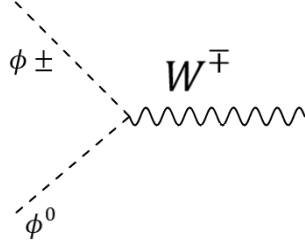


Figure 1. Feynman diagram depicting charged and neutral ϕ field components coupling with a W boson.

We note that at this level with L_0 couplings only, the lightest bi-adjoint mode is stable at tree level. We must assume further interactions for the lightest state to decay.

Both the real and complex bi-adjoint models allow for trilinear interactions between the ϕ components through the δ couplings. These trilinear interactions can induce effective dimension 5 couplings. There may also be additional sources of dimension 5 couplings.

We now add a new dimension 5 effective operator to the L_{0R} Lagrangian. This new operator allows the real bi-adjoint components to further interact with the Standard Model. At dimension 4, the $(8, 3, 0)$ bi-adjoint has no allowable couplings between individual components of ϕ and the SM. In particular, couplings to quark bilinears $\overline{Q}_L^c Q_L$, which would conserve color and weak charge, are forbidden by hypercharge conservation. Our new operator will thus introduce the lowest dimension effective interaction by which the lightest bi-adjoint could decay.

This new effective operator couples a single bi-adjoint scalar directly to the SU(2) and SU(3) field strength tensors. Our operator is

$$L = \frac{1}{\Lambda} \phi^{ij} W_{ij}^{\mu\nu} G_{\mu\nu} . \quad (7)$$

In Eq. 7, ϕ is the $(8, 3, 0)$ bi-adjoint. The Roman letters indicate SU(2) indices while Greek letters indicate Lorentz indices. $W^{\mu\nu}$ is the SU(2) field strength tensor and $G_{\mu\nu}$ is the SU(3) field strength tensor. Λ is the effective cutoff of the operator. We see that this operator has an effective dimension 5. After electroweak symmetry breaking, the SU(2) field strength tensor $W^{\mu\nu}$ will contain the W, Z, and γ electro-weak gauge fields. This model thus presents an unusual operator in W-gluon sector of the di-boson portal, the portal through which new particles interact with the SM primarily through pairs of SM gauge bosons.

Expanding the above operator in components, we extract the Lagrangian terms involving the charged bi-adjoints ϕ^\pm

$$\begin{aligned}
L \supset & (\partial^\mu A_3^\nu - \partial^\nu A_3^\mu)(\partial_\mu W_\nu^+ - \partial_\nu W_\mu^+) \phi^- + (\partial^\mu A_3^\nu - \partial^\nu A_3^\mu)(\partial_\mu W_\nu^- - \partial_\nu W_\mu^-) \phi^+ \\
& + eg_3 f^{abc} A_{3b}^\mu A_{3c}^\nu (\partial_\mu W_\nu^+ - \partial_\nu W_\mu^+) \phi_a^- + eg_3 f^{abc} A_{3b}^\mu A_{3c}^\nu (\partial_\mu W_\nu^- - \partial_\nu W_\mu^-) \phi_a^+ + \\
& \frac{iec_w}{s_w} (W_\mu^+ Z_\nu^0 - W_\nu^+ Z_\mu^0) (\partial^\mu A_3^\nu - \partial^\nu A_3^\mu) \phi^- + \frac{iec_w}{s_w} (W_\mu^- Z_\nu^0 W_\nu^- Z_\mu^0) (\partial^\mu A_3^\nu - \partial^\nu A_3^\mu) \phi^+ + \\
& - ie (W_\mu^+ A_\nu - W_\nu^+ A_\mu) (\partial^\mu A_3^\nu - \partial^\nu A_3^\mu) \phi^- + ie (W_\mu^- A_\nu - W_\nu^- A_\mu) (\partial^\mu A_3^\nu - \partial^\nu A_3^\mu) \phi^+. \quad (8)
\end{aligned}$$

We also find the Lagrangian terms involving the neutral bi-adjoints ϕ^0

$$\begin{aligned}
& s_W (\partial^\mu A_3^\nu - \partial^\nu A_3^\mu) (\partial_\mu A_\nu - \partial_\nu A_\mu) \phi^0 + c_W (\partial^\mu A_3^\nu - \partial^\nu A_3^\mu) (\partial_\mu Z_\nu - \partial_\nu Z_\mu) \phi^0 \\
& s_w g_3 f^{abc} A_{3b}^\mu A_{3c}^\nu (\partial_\mu A_\nu - \partial_\nu A_\mu) \phi^0 - c_W g_3 f^{abc} A_{3b}^\mu A_{3c}^\nu (\partial_\mu A_\nu - \partial_\nu A_\mu) \phi^0 + \\
& \frac{ie}{s_w} (W_\mu^+ W_\nu^- - W_\nu^+ W_\mu^-) (\partial^\mu A_3^\nu - \partial^\nu A_3^\mu) \phi^0. \quad (9)
\end{aligned}$$

In the Lagrangians above, A_3 are the gluon fields, W^\pm are the W boson states, and A is the photon. In the first line, we have direct three-point interactions between the ϕ^\pm and a $W^\mp g$ pair, shown in Fig. 2.

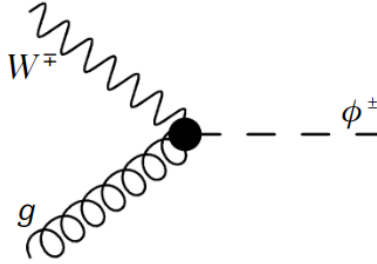


Figure 2. Feynman diagram depicting charged LEX ϕ^\pm coupling to a W boson and gluon.

This interaction allows the direct decay of a charged ϕ^\pm into a W-gluon resonance. It also allows a variety of new LHC production modes for charged bi-adjoints, as we will later see.

In Eq. 9, there is a similar three-point interaction for the neutral state ϕ^0 with one gluon and a neutral gauge boson (Z or γ), shown in Fig. 3.

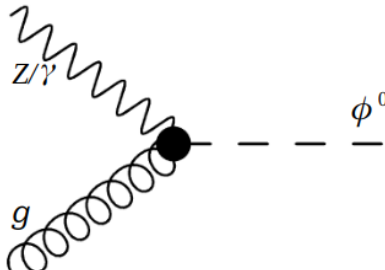


Figure 3. Feynman diagram depicting neutral LEX ϕ^0 coupling to a gluon and Z boson or photon.

This can allow the decay channel of a neutral state into a gluon-photon or gluon-Z resonance.

Starting on the second line of Eq. 8, there are triple gauge boson interactions. On the second line of Eq. 8, there are interactions that couple a single charged ϕ^\pm to a W boson and two gluons. In the third and fourth lines, we find interactions that couple the charged components of ϕ to one gluon, one W boson, and one neutral electroweak gauge boson (Z or photon). In Eq. 9, we find interactions that couple the neutral component ϕ^0 to various combinations of W bosons, neutral electroweak gauge bosons, and gluons. We represent these interactions as Feynman diagrams in Fig. 4.

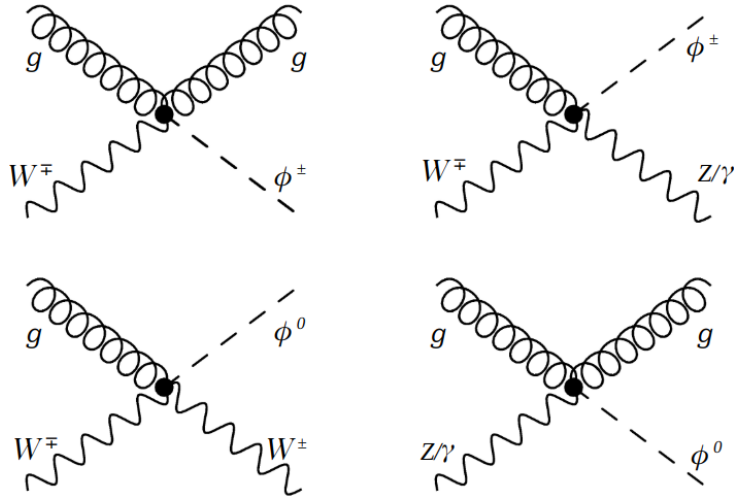


Figure 4. Feynman diagrams depicting an $(8, 3, 0)$ LEX scalar coupling to 3 gauge bosons..

The above interactions lead to a variety of interesting 2-2 and 2-3 collider production processes for the charged and neutral components of the bi-adjoint. In addition to these terms, the Lagrangian contains several 5-point interactions that couple the ϕ fields to 4 gauge bosons. These operators contribute to various 2-3 collider production processes that will not be the subject of this work.

The operator specified in Eq. 7 can be added to the dimension 5 theory as a stand-alone operator generated by higher-energy physics. It will also receive a contribution in the tree-level model, from a one loop triangle diagram involving the trilinear coupling of the adjoints, $\delta\phi^3$. We re-iterate that this is the lowest dimension effective operator through which the bi-adjoint can couple to the diboson portal; all other effective operators will require additional suppression by insertions of Higgs vevs to soak up $SU(2)$ indices.

We note that we may add an equivalent operator

$$L = \frac{1}{\Lambda} \phi_I^{ij} \tilde{W}_{ij}^{\mu\nu} G_{\mu\nu} , \quad (10)$$

which will allow similar interactions of the imaginary components of ϕ with the $SU(2)$ and $SU(3)$ field strength tensors. This will allow, for example, the decay of the pseudo-scalar states in the ϕ_I multiplet to decay to di-bosons pairs as well.

Parameter space benchmark

In this work, we are interested in analyzing some of the phenomenology of the simplest bi-adjoint model. We will thus choose to first analyze the real scalar model. As previously detailed, in this LEX bi-adjoint there are three states, components of the real adjoint, which are CP even spin zero scalars. Furthermore, the masses of these states are the same, $m_{\phi^+}^2 = m_{\phi^0}^2 = m_{\phi^-}^2$.

However, our conclusions will also apply to regions of the complex scalar model where the imaginary (pseudo-scalar) bi-adjoints are much heavier than the real (scalar) bi-adjoints and as such are not easily accessible to the LHC. Production of the pseudo-scalar states at the LHC can be achieved by moving their masses into the 6 - 7 TeV range, though their existence can still contribute to loop-level decays of the scalar states at any mass. In this region of the complex model space, we choose $\lambda_3 = \lambda_4 = 0$, which does not allow mass splitting between charged and neutral states and guarantees that mass eigenstates are of definite CP. We can thus choose values of $m^2 > 0$ and $M^2 < 0$ with $|m^2| > |M^2|$ to avoid developing a ϕ vev. A fine tuning of order 10 percent between mass parameters will deliver 1-4 TeV masses for scalar components while pseudo-scalars remain above the 7 TeV scale.

The Higgs couplings in both the real and complex models will induce one-loop enhancements of Higgs couplings to gluons and Higgs couplings to di-photons [27]. In the $(8, 2, 1)$ Manohar-Wise models, these effects appear to be compatible with Higgs production and decay measurements for exotic states above 1 TeV in mass for order one couplings [19, 28]. We expect similar results in our model. However, we can consider all Higgs couplings to be zero in our very simplest benchmark point, which means the bi-adjoints make no one-loop contributions to the Higgs di-boson couplings.

III. DECAYS OF THE BI-ADJOINTS

We now discuss the decay modes of the bi-adjoint components. The dimension 5 effective operator allows for a two-body resonant decay of the charged component to a W boson and a gluon: $\phi^\pm \rightarrow W^\pm g$. This decay will make up 100% of the branching fraction of the charged bi-adjoint if the mass splitting between the charged and neutral components is zero. The total decay width of the bi-adjoint will be proportional to a factor of $\Gamma \sim m_{\phi^\pm}^3/\Lambda^2$. In Fig. 5, we plot the decay width of the lightest charged bi-adjoint in the m_{ϕ^\pm}, Λ parameter plane.

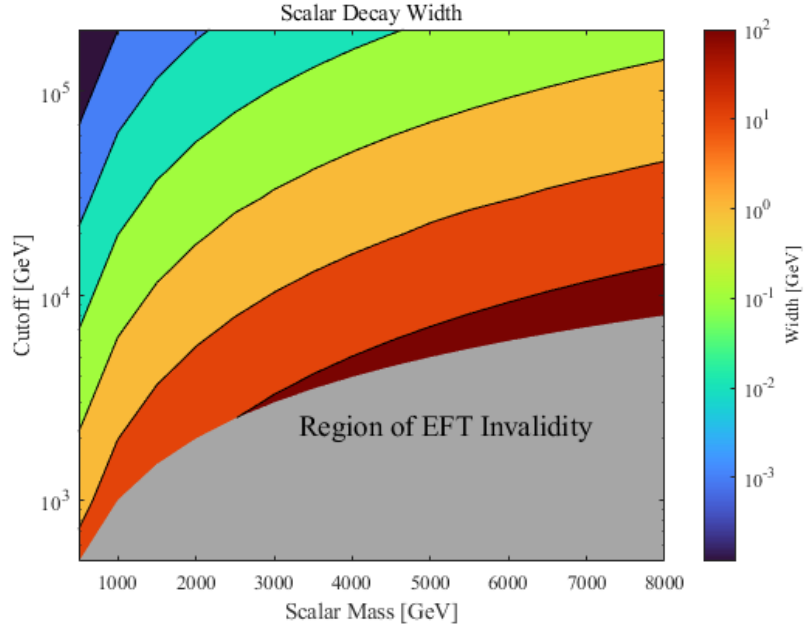


Figure 5. Decay width of the lightest ϕ^\pm in the Λ -scalar mass plane.

We note that the region of very low effective cutoff, $\Lambda < m_{\phi^\pm}$, the effective operator validity breaks down. Therefore, we see that the width increases at high mass and low effective cutoff but remains relatively narrow compared to the mass over the region of EFT validity.

The neutral component will always have available 2 body-decay modes of $\phi_0 \rightarrow \gamma g$ and $\phi_0 \rightarrow Zg$ through the effective operator. The relative decay widths of the gZ and $g\gamma$ decays are fixed by $SU(2)$ gauge invariance. In principle, the neutral component of the bi-adjoint can also develop a decay width into di-gluons at loop level. However, this requires two Higgs insertion to "soak up" $SU(2)$ indices. As such, this happens through an effective operator of dimension 7. This means that any digluon decay will be suppressed compared to decays of the neutral states that result from dimension 5 operators. In the real adjoint model, the di-gluon coupling happens through a one-loop process involving bi-adjoints in a triangle loop; however, two conditions must be met for this coupling to be non-zero. First, the trilinear coupling $\delta\phi^3$ must be non-zero. Second, the di-Higgs coupling must be non-zero. Similar gluon-Z, gluon-photon, and digluon couplings and decays were studied for a slightly different dimension 5 operator model coupling to a pure color adjoint $(8, 1, 0)$ in reference [11]. However, this model also allowed the dimension 5 decay of a color adjoint into gluons. Thus, the digluon decay took up a much more substantial fraction of the branching ratio. In the $(8, 3, 0)$ model without an appreciable gluon decay branching fraction, the branching ratio of the neutral state to Z -gluon vs γ -gluon decays is $\mathcal{B} \sim c_w^2/s_w^2$ for heavy states. The Z decays will dominate the branching fraction.

IV. LHC PRODUCTION MODES

We will now enumerate the most likely production modes for the $(8, 3, 0)$ bi-adjoint field at the LHC.

Pair Production

Hadron colliders can always pair-produce new states charged under the Standard Model gauge groups through gauge boson interaction terms that emerge from the exotic field's kinetic term. For color-charged particles, the largest pair production cross section is from gluon fusion. In our case, the production processes are $gg \rightarrow \phi^0\phi^0, \phi^+\phi^-$. In Fig. 6, we present the Feynman diagrams involved in the gluon fusion pair production of the bi-adjoint scalars.

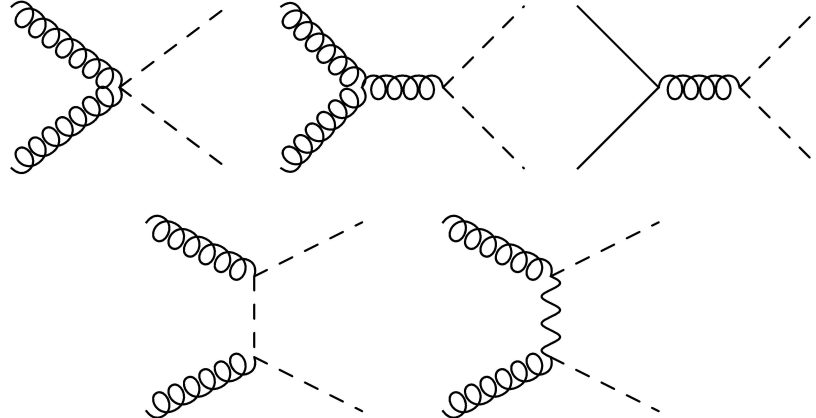


Figure 6. Pair Production modes of the $(8, 3, 0)$ bi-adjoint.

We note that the new trilinear electroweak-gluon- ϕ^\pm vertex from the dimension 5 operator also makes a contribution to the gluon fusion pair production through t-channel W exchange. This is the bottom right diagram in Fig. 6.

Single Production of Charged Bi-Adjoint Scalars

We will now explore the single production modes of bi-adjoints at the LHC. The effective dimension 5 operator allows a variety of single production modes for the charged and neutral bi-adjoint components. Here we will concentrate on the most probable 2-2 LHC processes in which a single bi-adjoint is produced in association with one SM particle. We will first focus on the production of the charged ϕ^\pm states. Fig. 7 displays single-production modes of the lightest charged bi-adjoint, along with its subsequent decay back into a W-gluon resonance.

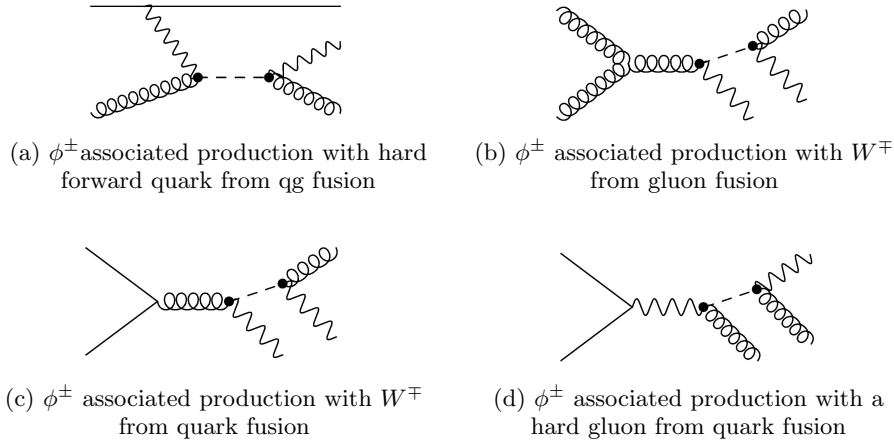


Figure 7. Single Production modes of the charged $(8, 3, 0)$ bi-adjoint at the LHC, with subsequent decay $\phi^\pm \rightarrow W^\pm g$.

Gluon Fusion

The first production mode that we will discuss is the gluon fusion mode, where a single charged ϕ^\pm is produced with an associated W boson. Diagrams contributing to this process follow from the three-point W-g- ϕ vertex and

4-point $ggW\phi$ vertices of the dimension 5 operator. One of the gluon fusion diagrams is shown in Fig. 7b, which depicts the process $gg \rightarrow W^\pm\phi^\mp$. Once ϕ^\mp decays, events in this channel fall into 4 $W^\pm(W^\mp g)$ final states where there is one resonance (Wg).

Quark Fusion

There are two possible LHC quark fusion processes that produce a single charged ϕ^\pm . The first process is quark fusion with $W\phi$ associated production, shown in Fig. 7c. The full process is $q\bar{q} \rightarrow g^* \rightarrow W^\pm\phi^\pm$. In this process, same flavor quarks fuse into an off-shell gluon, and a $W^\pm\phi^\pm$ pair is created through the trilinear $W\text{-}g\text{-}\phi^\pm$ effective vertex. Once the ϕ^\pm decays, the final state topologies are again $W^\pm(W^\mp g)$, where the W 's have either di-quark or lepton neutrino decay patterns.

The second quark fusion process produces a single ϕ^\pm in association with a hard gluon. This is illustrated in Fig. 7d. The full process is $q\bar{q}' \rightarrow W^{\pm*} \rightarrow g\phi^\pm$. In this process, a $q\bar{q}'$ pair fuse into an off-shell W boson which produces a final state gluon- ϕ pair through the 3-point $W\text{-}g\text{-}\phi$ dimension 5 effective vertex. Once the ϕ^\pm decays, the final state is $q\bar{q} \rightarrow g(W^\pm g)$, where the W and one hard gluon jet form a mass resonance. The subsequent decay of the W into jj or $\ell\nu$ pairs gives 4 final state topologies.

Quark-Gluon Fusion

The final single production mode is an interesting asymmetric process which produces a ϕ^\pm in association with a hard forward quark jet. This process can be seen in Fig. 7a. In this t-channel quark-gluon fusion process, the initial state gluon fuses with an off-shell W radiated by the incoming quark. The three-point $W\text{-}g\text{-}\phi$ vertex produces a single ϕ in addition to the hard forward quark. The process is written as $qg \rightarrow q'\phi^\pm$. Once the ϕ^\pm decays to a W -gluon resonance, the process is $qg \rightarrow q'(W^\pm g)$, where the W and the hard gluon form a resonance. With W decaying to di-jets or lepton-neutrino pairs, there are two final-state event topologies.

Cross Section Comparison

We have plotted comparisons of various charged ϕ^\pm production cross sections for the 14 TeV LHC. To produce these cross sections, we have used FEYNRULES [29, 30] to implement Lagrangian interactions from Section 2 and generate UFO output [31]. We then used MADGRAPH5_AMC@NLO (MG5_AMC) [32] to generate cross sections for five different production processes. These include pair production from gluon fusion and four single production channels, $qg \rightarrow \phi q$, $gg \rightarrow \phi W$, $qq \rightarrow \phi W$, and $qq \rightarrow \phi g$. These processes are all depicted in Figs. 6 and 7. In Fig. 8, we plot the cross sections for these processes at different bi-adjoint masses, using a benchmark choice of effective cutoff $\Lambda = 5$ TeV.

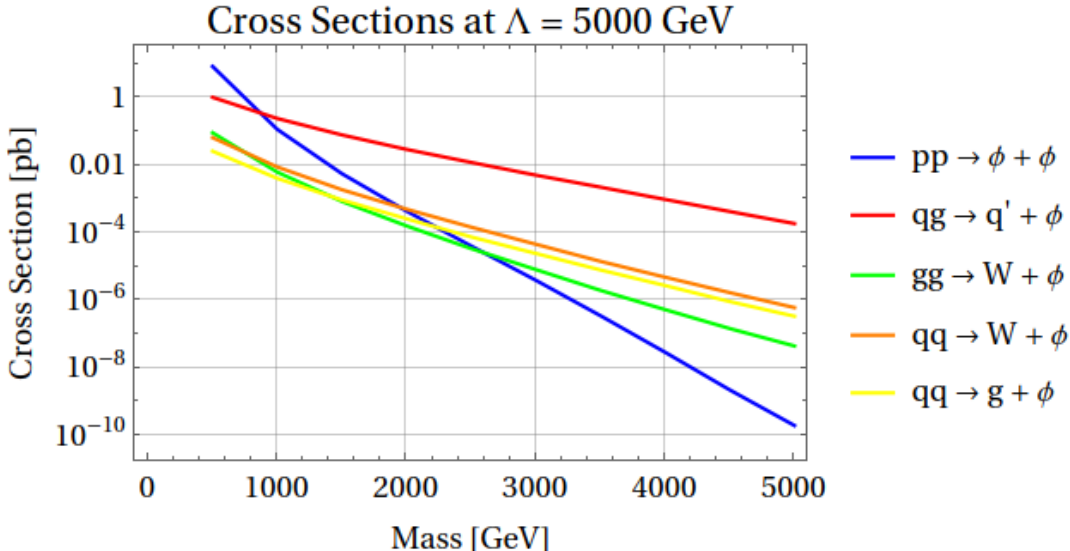


Figure 8. Comparison of the cross section vs ϕ^\pm mass for 5 production processes. We use the values $\Lambda = 5$ TeV and $m_{\phi^+} = m_{\phi^-}$.

We find that the pair production cross section only dominates over single production for low masses of ϕ around 800 GeV. This pair production cross section drops off somewhat dramatically as the scalar mass increases due to the kinematic suppression of two high-mass final-state particles. For a 10 TeV effective cutoff, we find a similar feature with single production taking over just after the 1 TeV threshold. The single production modes maintain more kinematic phase space at high bi-adjoint mass, so for most of the multi-TeV parameter space, single production processes have the leading cross sections.

The single production mode that clearly dominates is the quark-gluon fusion process $gq \rightarrow q' + \phi$, which fuses an off-shell W with the incoming gluon. This cross section beats those of the other single production modes at all masses and cutoffs tested. We note that in the quark-gluon fusion channel, single production cross sections of the bi-adjoint remain above the fb range for 3-4 TeV particle masses.

In addition to the difference in cross sections, we expect this single production mode involving a radiated boson to create a distinctive, asymmetric signal at the LHC due to a massive ϕ^\pm and a hard forward jet. These events will also have a distinctive W-gluon resonant feature. Due to these reasons, we will propose a single production HL-LHC search in this channel later in the paper.

Neutral States

Single production modes for the neutral gauge boson are similar to those involving the charged gauge boson, but with neutral Z and γ electroweak bosons appearing in the final states rather than W bosons. We give a schematic of the LHC single production modes in Fig. 9.

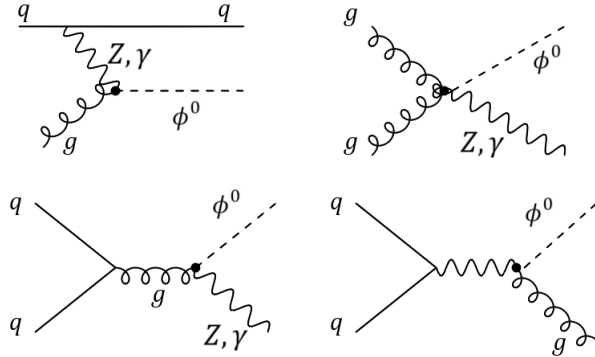


Figure 9. LHC single production modes of neutral bi-adjoints

The gluon fusion mode leads to the production of a ϕ^0 in association with a final state Z or γ through the process $gg \rightarrow \phi^0 + Z/\gamma$. An example diagram is shown in Fig. 9b. Quark fusion also yields $\phi^0 Z$ and $\phi^0 \gamma$ final states through quark fusion into an off-shell gluon. This is demonstrated in Fig. 9c with the process $q\bar{q} \rightarrow g^* \rightarrow \phi^0 + Z/\gamma$. Separate quark fusion processes yield a $\phi^0 g$ final state through quark fusion into an off-shell Z or γ in Fig. 9d. Finally, the t-channel quark-gluon process gives a $\phi^0 + q$ final state as an incoming gluon fuses with a neutral gauge boson radiated off of the initial state quark. This process is shown in Fig. 9a and is $qg \rightarrow q + \phi^0$. The production processes are generally smaller for neutral bi-adjoints than for the charged states, especially the quark and gluon associated production processes which contain off-shell photons and Z's. Still, there are several promising LHC signatures with final-state photons, such as the gluon fusion process $gg \rightarrow \gamma\phi^0 \rightarrow \gamma(g\gamma)$.

V. LHC SEARCH FOR CHARGED BI-ADJOINTS

In this section, we propose a new HL-LHC search for the single production of the charged bi-adjoint field. This search makes use of the most probable single production mode for ϕ^\pm and its distinctive W-gluon resonant decay. We propose a search in the quark-gluon fusion channel where ϕ^\pm is produced in association with a hard forward jet. The ϕ^\pm then decays to a W-gluon resonance with the total process $qg \rightarrow q' \phi^\pm \rightarrow W^\pm g + j$. Finally, for our search, we will consider leptonic decays of the bi-adjoint: $\phi^\pm \rightarrow Wg \rightarrow \ell^\pm \nu g + q$. The full process is then

$$qg \rightarrow q' \phi^\pm \rightarrow W^\pm g + j \rightarrow \ell^\pm \nu g + q .$$

This is a quite probable final state for the search, as the leptonic branching fraction of the W is ~ 20 percent. In Fig. 10 below, we show the Feynman diagram of the total production and decay for this process.

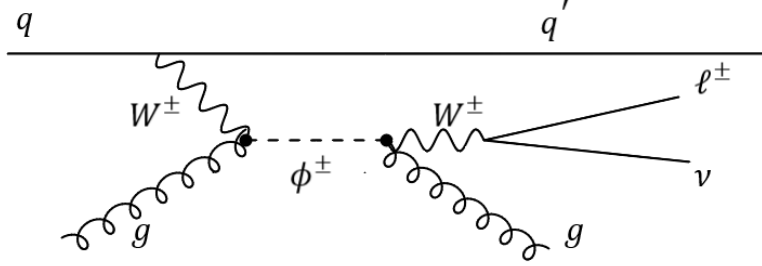


Figure 10. Associated production of ϕ^\pm and forward jet with subsequent decay $\phi^\pm \rightarrow W^\pm g \rightarrow \ell^\pm \nu g$

There are many distinctive features of this process. First, it contains both missing energy and a single hard lepton. It has a hard forward jet. It also has a very hard gluon jet emanating from the decay of the potentially multi-TeV ϕ particle. The characteristic p_T of this gluon jet peaks at about half of the ϕ mass. Finally, the leading jet and lepton have a transverse mass that has a kinematic edge at the mass of the ϕ^\pm particle.

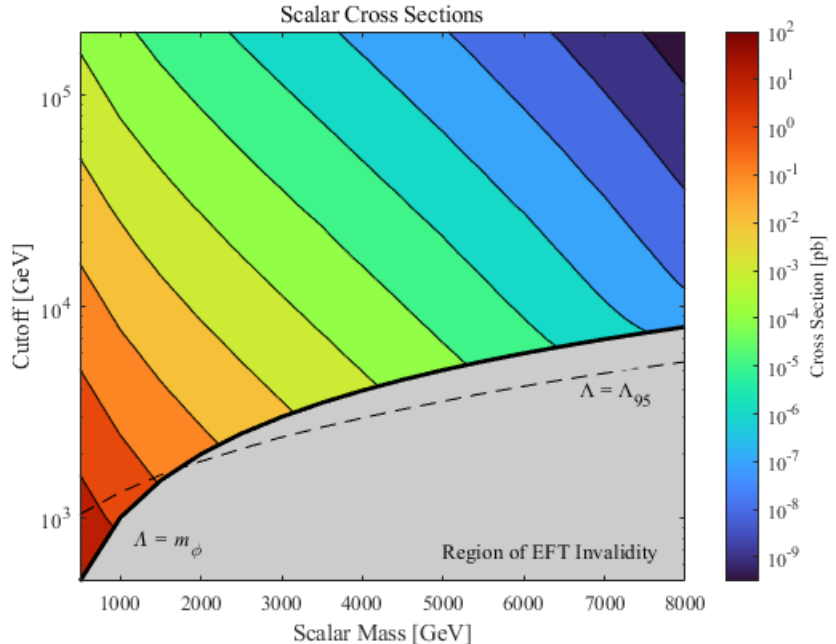


Figure 11. Combined cross sections for the single production channel $qg \rightarrow q + \phi^\pm$ in the m_{ϕ^\pm}, Λ plane. We note the regions $\Lambda < m_{\phi^\pm}$ and $\Lambda < \Lambda_{95}$ where the EFT becomes invalid.

In Fig. 11, we show a contour plot of production cross sections at the 14 TeV LHC for the $qg \rightarrow \phi^\pm q'$ process in the m_{ϕ^\pm}, Λ mass plane. Cross sections are computed with MG5_AMC and scaled by a modest k-factor of 1.3. This k-factor is in the lower range of those found for QCD processes similar to that of our signal, and as such can reasonably be used. In these simulations, we use a simple benchmark model scenario where the charged bi-adjoint is a CP-even scalar, $m_{\phi^+} = m_{\phi^-}$, and charged bi-adjoints have a W -gluon pair as their only decay mode. In Fig. 11, we have displayed two different estimates that may be used for the region of operator invalidity. The first of these, $\Lambda < m_\phi$, assumes that the cutoff scale should correspond to the scale of the ultraviolet degrees of freedom. This choice is shown by the bold solid black line, and all values which do not satisfy this bound are shown in grey. The second choice which we display, $\Lambda = \Lambda_{95}$, is denoted by the dashed black line. This cutoff has been calculated using the s-matrix unitarity bound, as detailed in [3] and [33]. Specifically, we used the matrix element to find the limit

$$\Lambda \geq \frac{g\sqrt{\hat{s}}}{16\pi} \left(1 - \frac{m_\phi^2}{\hat{s}}\right) \left[1 + \frac{2m_\phi^2}{\hat{s} - m_\phi^2} - \frac{2m_\phi^2 m_W^2}{(\hat{s} - m_\phi^2)^2} \ln \left(1 + \frac{\hat{s} - m_\phi^2}{m_W^2}\right)\right], \quad (11)$$

where \hat{s} is the partonic center-of-mass energy. Using our event samples generated by MG5_AMC, in conjunction with MADANALYSIS 5 [34], we were able to find cutoff values such that at least 95% of our signal events would satisfy the limit given in Eq. 11. It is this limit, which we call Λ_{95} , that is also displayed in Fig. 11; though not marked in grey, all values under this line should also be considered invalid.

In Fig. 11 we see, of course, that the production cross section falls off with increasing scalar mass. The overall production cross section falls as $1/\Lambda^2$. However, we maintain appreciable LHC production cross sections for quite massive ϕ^\pm , into the 4 TeV range. Production cross sections also remain appreciable for effective cutoffs in of order 10s of TeV. In Fig. 11 we have again noted the region of low effective cutoff, $\Lambda < m_{\phi^\pm}$, where the EFT becomes invalid.

Our goal is to institute a sensitivity study for the single bi-adjoint production channel $qg \rightarrow \phi^\pm + q' \rightarrow \ell^\pm \nu g + q'$ for the complete 3 ab^{-1} run of the HL-LHC. To obtain our signal events, we implemented the Lagrangian in Section 2 with FEYNRULES and output UFO files to MG5_AMC for event generation. We then showered the events with PYTHIA 8 [35] and passed them into MADANALYSIS 5 for detector simulation and object reconstruction, using the inbuilt simplified fast detector simulator (SFS) [36] and FASTJET [37]. In this, we use the default settings, including the use of an anti- k_T algorithm [38]. We set the radius parameter to $R = 0.4$.

Based on the expected kinematics of the signal and the need to limit the number of background events required, we implemented a few pre-selection criteria on both the signal and background events. We require at least two hard jets, exactly one hard lepton, and significant missing energy in our events. We institute the following pre-selection search criteria.

Pre-selection Criteria

- Events must have 2 hard jets: $p_T > 30 \text{ GeV}$
- Events must contain significant missing energy: $E_T^{\text{miss}} > 70 \text{ GeV}$
- Events must contain exactly one hard isolated lepton: $p_T > 10 \text{ GeV}$

The leading backgrounds for this process are $t\bar{t}$ and $W + \text{jets}$ with leptonic decay of the W . Other important backgrounds include the di-boson processes $WW/ZZ/WZ$. Smaller but still significant backgrounds include the asymmetric processes of qt and Wt production.

In Table I, we list background production cross sections for the 5 background processes for 14 TeV c.o.m. energy at the LHC. Background events were created similarly to the signal: events were generated with Madgaph5@NLO and showered with PYTHIA 8 [35]. The events were run through the SFS and FASTJET detector simulation and reconstruction, again on default settings with the radius parameter set to $R = 0.4$. The background cross sections were computed at leading order with MG5_AMC, including a 70 GeV missing energy pre-selection threshold, and scaled by the listed k-factors in Table I. This table also lists the number of events of each background type that were generated.

Background Process	Cross Section (pb)	K-Factor Used	Events Generated
$t\bar{t}$	888.78	1.489	1150k
$W + \text{jets}$	1361	1.401, 1.234	1850k
Diboson	441.7	1.417, 1.316, 1.599	500k
qt	51.84	1.29	400k
tW	91.742	1.4	200k

TABLE I: Leading order cross sections in 5 background channels generated by MG5_AMC. These are scaled by appropriate k-factors, found in [39]. A preselection cut of $\text{MET} > 70$ was applied in event generation.

In order to justify our choice of selection cuts, we created kinematic distributions for several discriminants in our LHC process. This distribution binning, and the following analysis, were created using MADANALYSIS 5 and the previously described signal and background samples.

We start by examining a few transverse momentum distributions. In Fig. 12 below, we plot p_T distributions for the two leading jets in the signal and background events. Signal events are plotted for four ϕ^\pm mass benchmarks of 500 GeV, 1 TeV, 3 TeV, and 5 TeV.

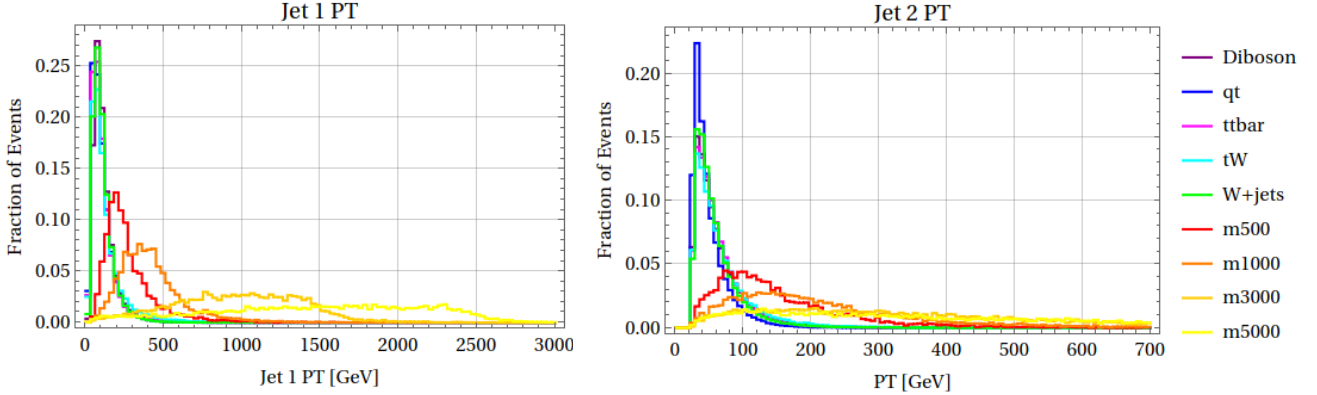


Figure 12. Plots of transverse momentum distributions in 14 TeV LHC $qg \rightarrow \phi^\pm + q$ events. There are plots of this kinematic variable for both the leading jet (left) and the sub-leading jet (right). Distributions are made with four benchmark ϕ^\pm masses.

In the signal events the leading jet, most likely the gluon emanating from the two-body decay of the ϕ^\pm , has a characteristic peak around half of the ϕ^\pm mass. This characteristic p_T becomes extremely substantial at high ϕ^\pm mass. The transverse momentum of the sub-leading jet, the associated quark jet, remains characteristically lower over a large range of ϕ^\pm masses. This jet is forward and has small component in the transverse direction. However, the characteristic peak for this jet occurs in the hundred GeV range for low masses, but becomes substantially distributed over a few hundred GeV range for high-mass bi-adjoint events. By contrast, the leading and sub-leading jets in the background both peak at extremely low momentum and do not extend substantially into the few hundred GeV range.

Next, we have plotted the missing energy distributions of signal and background events in Fig. 13. The plots show the missing energy vs. the fraction of events on both logarithmic and linear scales. Signal events were again plotted at four mass benchmarks of 500 GeV, 1 TeV, 3 TeV, and 5 TeV.

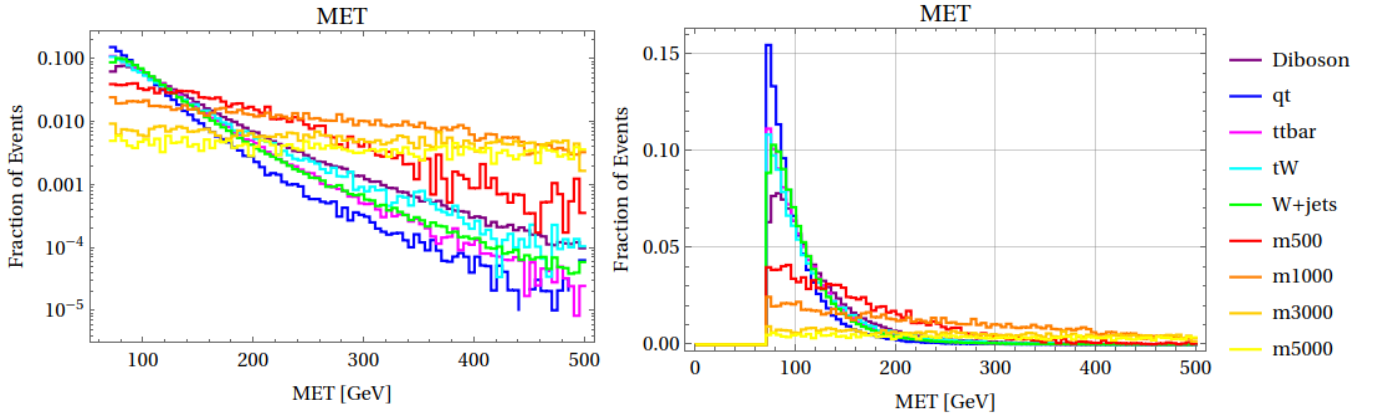


Figure 13. Plots of missing energy distributions for signal and background events at 14 TeV LHC. There is a logarithmic-scale plot (left) and a linearly scaled plot (right). Distributions are made with four benchmark ϕ^\pm masses.

The signal events have a greater event fraction than the background at higher missing energy thresholds. The fraction of events occurring at high missing energy increases with increasing bi-adjoint mass. The qt , $ttbar$, and tW backgrounds are monotonically decreasing, while the diboson and $W+jets$ backgrounds peak at low MET thresholds and dramatically fall, with all backgrounds very suppressed for missing energies above 140 GeV.

We also plot the transverse mass distribution of the leading jet-lepton pair. We again plot the distribution for signal and background events, using the same four benchmark ϕ^\pm masses.

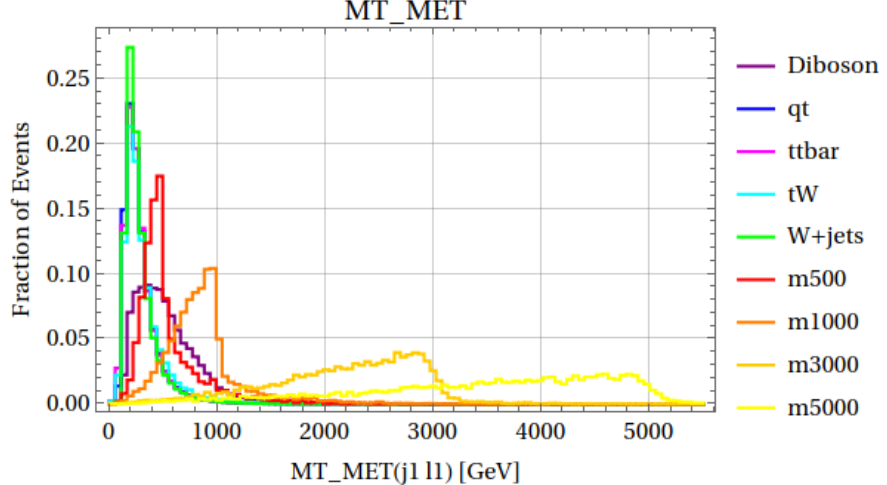


Figure 14. Plot of the leading jet-lepton transverse mass distribution for signal and background events at 14 TeV LHC. Distributions are made with four benchmark ϕ^\pm masses 500 GeV, 1 TeV, 3 TeV, and 5 TeV.

We see that the signal events display a kinematic peak and edge at a transverse mass threshold corresponding to the bi-adjoint mass. The high-mass signal events are noticeably flatter than low-mass events, with smearing of the edge, but the feature is still easily discernible. The backgrounds, with the notable exception of the di-boson background, peak around the 100 GeV threshold. The diboson background peaks at a slightly higher threshold, significantly overlapping with the 500 GeV signal events.

Finally, we plot lepton p_T distributions for the signal and backgrounds in Fig. 15. We use the same choice of signal masses as in Fig. 12-14.

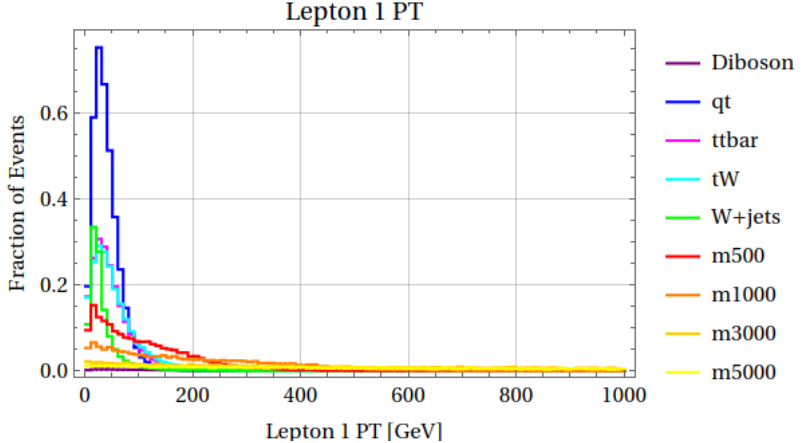


Figure 15. Plot of the lepton p_T distribution for signal and background events at 14 TeV LHC. Distributions are made with four benchmark ϕ^\pm masses 500 GeV, 1 TeV, 3 TeV, and 5 TeV.

We see that while both signal and background lepton p_T peaks at low momentum, there is an appreciable spread of higher p_T lepton events in the signal samples. The lepton p_T distribution of the signal events shows a considerable flattening for higher bi-adjoint masses.

Search Criteria

With the knowledge of our kinematic distributions, we can impose further cuts. Due to the differences between the distributions for different masses, we choose to create low-, medium-, and high-mass search regions. These search regions include thresholds for the reconstructed transverse mass of the leading jet-lepton pair, $m_{T,j_1\ell}$. They also include an increasing p_T threshold for the leading and sub-leading jets.

In the low mass region we require

- $E_T^{miss} > 140$ GeV

- p_T leading jet > 180 GeV
- p_T sub-leading jet > 85 GeV
- $m_{T_{j_1\ell}} > 700$ GeV

In the intermediate mass region we require a slightly higher threshold for the leading and sub-leading jets. In this intermediate region, we also use a sliding window of transverse mass thresholds for the leading jet-lepton pair that cuts the region into 6 bins. The requirements for this region follow.

- $E_T^{\text{miss}} > 140$ GeV
- p_T leading jet > 200 GeV
- p_T sub-leading jet > 110 GeV
- $m_{T_{j_1\ell}}$ in 6 bins between > 1100 and > 2350 GeV

In the high mass region we use a single stringent high mass threshold on the transverse mass.

- $E_T^{\text{miss}} > 1400$ GeV
- p_T leading jet > 200 GeV
- p_T sub-leading jet > 110 GeV
- $m_{T_{j_1\ell}} > 2400$ GeV

We will now show the efficiencies, or fraction of events remaining after each cut, of our search criteria for signal and background events. In Table II below, we give the cumulative cut flows for signal events in the bi-adjoint search. The table shows the cut-flows for the low, medium, and high mass search ranges. We give efficiencies of each selection cut for various ϕ^\pm mass values. The efficiencies in the low and high mass search regions follow the general pattern of increasing with increasing bi-adjoint mass. In the the low search region, the lightest mass events are worse at passing the 140 GeV missing energy cut and transverse mass threshold. Efficiencies in the tighter $m_{T_{j_1\ell}}$ -binned medium-mass search region hold steady with an overall efficiency in the low 30 percent range. Signal events in the high mass search region do better at passing the 2.4 TeV transverse mass threshold as the bi-adjoint mass is increased.

Low Mass Region, $\sqrt{s} = 14$ TeV, labeled by m_Φ [GeV]

Selection criterion	500	750	1000	1250
$E_T^{\text{miss}} > 140$	0.292	0.447	0.529	0.604
$p_T(j_1) > 180$ GeV	0.251	0.396	0.496	0.580
$p_T(j_2) > 85$ GeV	0.171	0.337	0.435	0.522
$m_{T_{j_1\ell_1\text{MET}}} > 700$ GeV	0.0614	0.161	0.336	0.462

Mid-mass Region, $\sqrt{s} = 14$ TeV, labeled by m_Φ [GeV]

Selection criterion	1500	1750	2000	2250	2500	2750
$E_T^{\text{miss}} > 140$	0.6477	0.68416	0.7214	0.7401	0.7651	0.7843
$p_T(j_1) > 200$ GeV	0.6188	0.6586	0.6979	0.7187	0.7438	0.76258
$p_T(j_2) > 110$ GeV	0.5307	0.5689	0.6127	0.6350	0.65688	0.68241
$m_{T_{j_1\ell_1\text{MET}}} [\text{GeV}]$	1100	1300	1500	1650	1850	2350
Final $m_{T_{j_1\ell_1\text{MET}}}$ cut	0.328818	0.3305	0.3443	0.363416	0.35746	0.23568

Light Cuts, $\sqrt{s} = 14$ TeV, Background Efficiencies					
Selection criterion	t \bar{t}	W+jets	Diboson	qt	tW
$E_T^{\text{miss}} > 140$	0.0369	0.144	0.231	0.0267	0.0434
$p_T(j_1) > 180$ GeV	0.00954	0.0585	0.0852	0.0125	0.0167
$p_T(j_2) > 85$ GeV	0.0049	0.0271	0.0411	0.00166	0.0082
$m_{T_{j_1 l_2 \text{MET}}} > 700$ GeV	0.00103	0.00732	0.00267	0.000556	0.00252

Mid- and High-Mass Cuts, $\sqrt{s} = 14$ TeV, Background Efficiencies					
Selection criterion	t \bar{t}	W+jets	Diboson	qt	tW
$E_T^{\text{miss}} > 140$	0.0369	0.144	0.231	0.0267	0.0434
$p_T(j_1) > 200$ GeV	0.00766	0.0467	0.0677	0.0104	0.0144
$p_T(j_2) > 110$ GeV	0.00303	0.0172	0.0259	8.98e-04	0.00537
$m_{T_{j_1 l_1 \text{MET}}} > 1100$ GeV	1.69e-04	0.00133	3.96e-04	9.50e-05	6.42e-04
$m_{T_{j_1 l_1 \text{MET}}} > 1300$ GeV	8.01e-05	6.52e-04	2.06e-04	4.40e-05	4.09e-04
$m_{T_{j_1 l_1 \text{MET}}} > 1500$ GeV	4.14e-05	3.49e-04	1.21e-04	2.39e-05	2.16e-04
$m_{T_{j_1 l_1 \text{MET}}} > 1650$ GeV	2.02e-05	2.06e-04	7.77e-05	1.80e-05	1.67e-04
$m_{T_{j_1 l_1 \text{MET}}} > 1850$ GeV	9.22e-06	1.15e-04	4.61e-05	1.20e-05	1.40e-04
$m_{T_{j_1 l_1 \text{MET}}} > 2350$ GeV	2.77e-06	2.00e-05	1.43e-05	6.25e-06	2.07e-05
$m_{T_{j_1 l_1 \text{MET}}} > 2400$ GeV	1.84e-06	2.00e-05	1.07e-05	3.02e-06	2.07e-05

TABLE III: Efficiencies of the backgrounds after cuts for each region.

High Mass Region, $\sqrt{s} = 14$ TeV, labeled by m_Φ [GeV]					
Selection criterion	3000	3500	4000	4500	5000
$E_T^{\text{miss}} > 140$	0.7899	0.8199	0.8327	0.8496	0.8640
$p_T(j_1) > 200$ GeV	0.7701	0.8002	0.8074	0.8275	0.8375
$p_T(j_2) > 110$ GeV	0.6830	0.7110	0.7206	0.7385	0.7456
$m_{T_{j_1 l_1 \text{MET}}} > 2400$	0.2952	0.4373	0.5252	0.5826	0.6240

TABLE II: Cut-flows for signal samples in proposed search for scalar bi-adjoint. For each ϕ mass, cumulative efficiencies after each selection cut are listed. Results apply to center-of-mass energy $\sqrt{s} = 14$ TeV.

Efficiencies for the $t\bar{t}$, W +jets, diboson, qt, and tW backgrounds are found in Table III. The upper table presents cut flows for all 5 backgrounds in the low-mass search region. The lower table presents the intermediate mass and high mass search regions. In the low mass search region, final background efficiencies for the leading backgrounds are in the .1 percent range. In the intermediate and high mass search regions, the transverse mass cut is extremely powerful for suppressing the backgrounds, with W plus jets suppression of order 10^{-5} .

Implementing these search criteria for the full 3ab^{-1} data set for the HL-LHC, we compute the significance as

$$S = \frac{N_{\text{signal}}}{\sqrt{N_{\text{bkg}}}} . \quad (12)$$

We use the statistical uncertainty of the background as the uncertainty. In Fig. 16, we plot the $3ab^{-1}$ HL-LHC 5σ (blue) discovery potential and 2σ (red) sensitivity in the m_{ϕ^\pm} , Λ plane. Note that exclusions apply to the regions of EFT validity in the parameter space where $\Lambda > m_{\phi^\pm}$, or where the effective cutoff is greater than m_{ϕ^\pm} . This is roughly the minimum allowable center of mass energy of the events.

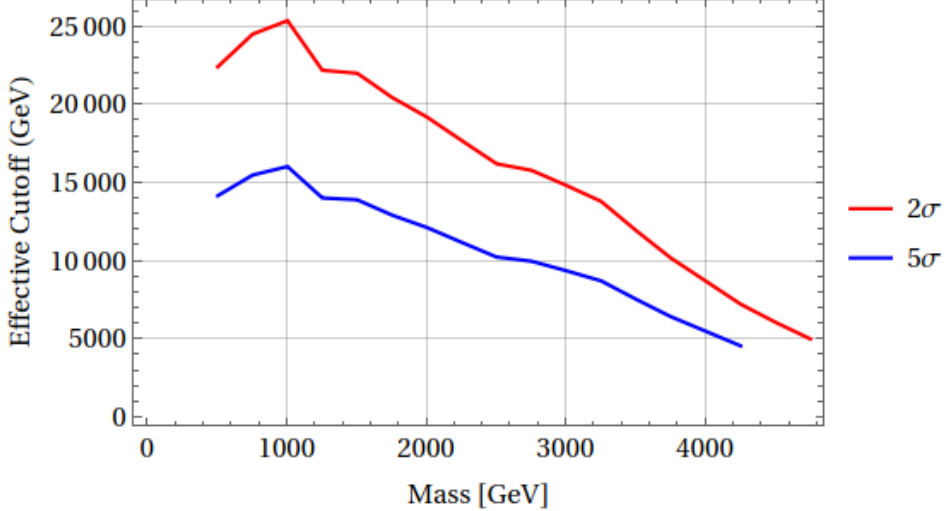


Figure 16. 5σ discovery potential and 2σ exclusions for charged bi-adjoints ϕ^\pm in $3ab^{-1}$ at HL-LHC.

The 5σ reach of the HL-LHC extends to 3-TeV bi-adjoints with effective cutoffs near the $\Lambda = 10$ TeV range. Discovery potential extends up to 4 TeV for $\Lambda = 5$ TeV, although this heavier region is near the limit of the effective operator paradigm. The 2σ sensitivity potential extends up to 19 TeV effective cutoffs for 2 TeV bi-adjoint masses and around 15 TeV effective cutoffs for 3 TeV bi-adjoint masses. The 2σ sensitivity extends to effective cutoffs of 5 TeV for 4.75 TeV bi-adjoints.

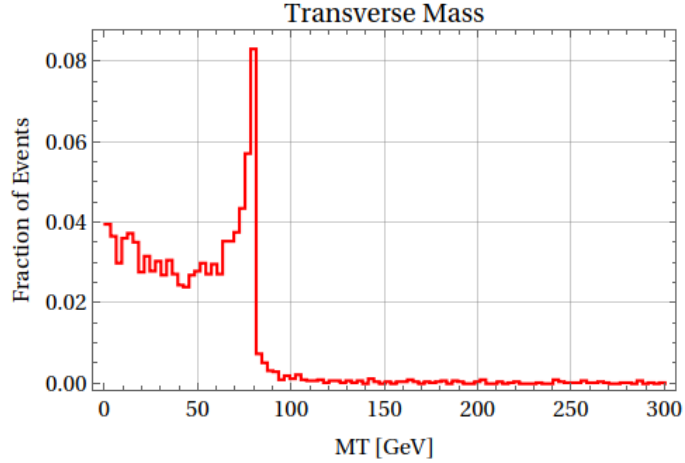


Figure 17. Transverse mass distribution for our charged bi-adjoint pair production signal.

We tested our LEX bi-adjoint model against previous searches at the LHC, to check that our search would contain better sensitivity to this exotic state. Specifically, we identified ATLAS-SUSY-2014-10 as a search that was likely to have sensitivity to our model [40, 41]. These searches are in the di-lepton, multi-jet plus MET channels. We used the previously-mentioned UFO files created through FEYNRULES to generate events involving pair-production of the charged ϕ^\pm states in MG5_AMC. The ϕ^\pm states were allowed to decay through our dimension-5 operator, and events were showered with PYTHIA 8 while the SFS with FASTJET detector simulation was again used with default settings. MADANALYSIS 5 was then used to re-implement the search. However, this search displayed no sensitivity to our new LEX state. A similar but more recent search, [42] demanded a single isolated lepton, vetoing events with more than one lepton. [42] also placed bounds on the transverse mass of the missing transverse momentum and lepton transverse momentum. While there is no public recast of this search available, we explored its potential for sensitivity to our

LEX state by implementing several of the cuts on our sample. This search is not sensitive to our bi-adjoint pair production process due to the cut on the transverse mass. Specifically, on the signal proposed in [42], the transverse mass distribution extended well beyond the W boson mass. However, the background distribution of transverse mass had an upper endpoint at the W boson mass. As displayed in Fig. 17, our signal process has an upper endpoint around the W boson mass, leading the transverse mass cut to exclude most of our signal. This graph is for a LEX mass of 500 GeV, but a very similar distribution results from all LEX masses. This lack of sensitivity is exciting, because it is indicative that this bi-adjoint, and other similar LEX states with larger SU(2) and SU(3) charges and asymmetric production processes, truly are relatively unexplored and still have significant discovery potential.

Other sources of constraint on these models might come from studies of the electroweak precision parameters. As the biadjoint generally contains charged and neutral states, one can compute the effects on the S and T parameters. In fact the author studies such effects in a bi-adjoint model [43]. Though the T parameter is sensitive to the mass splittings between the bi-adjoint charged and neutral states, we find general 2 sigma level compatibility in the fit to S and T parameters for mass splittings up to 100 or so GeV and masses in the TeV range(figure 4 in that work).

VI. CONCLUSIONS

We have explored several new LHC production modes for a CP-even exotic scalar which is a bi-adjoint under the Standard Model SU(3) and SU(2) symmetries, and where the field couples to the SU(2) and SU(3) field strength tensors through a new dimension 5 effective interaction. We have shown how single production of this exotic state is the dominant collider production mode for masses above a TeV and cutoffs in the 10 TeV range. We have explored the LHC production cross sections of this state in single production channels from both quark and gluon fusion. We have also introduced a new search in an asymmetric W-gluon fusion production channel where a single ϕ is produced in association with a hard forward jet. We showed how this production channel is the dominant production mode of the charged ϕ states and introduced a new HL-LHC search for a scalar produced in this mode with a decay to a gluon-W resonance. We found 5-sigma discovery potential for scalar masses up to 3 TeV with cutoffs of 10 TeV. We also found two-sigma sensitivity for masses up to 3 TeV with effective cutoffs around 15 TeV, and 4.75 TeV masses with 5 TeV cutoffs.

There are several new directions that could be pursued to follow up on this work. Most interesting would be a deeper phenomenological analysis of the complex bi-adjoint model. 1-4 TeV pseudoscalar states will generally have high LHC production cross sections [44]. In particular, it would be interesting to explore cascade decays in different mass-splitting regions of the parameter space. This would be especially interesting in regions where a pseudo-scalar sector is kinematically accessible. It would also be interesting to explore a full effective operator catalog for the bi-adjoint to see if other couplings to the Standard Model are possible with alternate phenomenology. Further precision analysis of this parameter space may yield interesting results for Higgs production and decay as well as for electroweak precision. In fact, the authors were successful in fitting recently fashionable electroweak parameters with other exotic color charged particles [43]. Other avenues of further study involve building UV completions of the dimension 5 operator that couple the bi-adjoint to the Standard Model.

It would also be interesting to use the W-gluon fusion process we have explored as a search channel for other exotic states that could be accessed through the W-gluon portal. These would include the $(8, 2, 1)$ Manohar-Wise field and the $(8, 4, -1)$ SU(2) quadruplet field. These states also have a varied phenomenology with various mass hierarchy regimes between field components, and interesting possibilities for cascade decays.

Appendix: Quartic Interactions of the Bi-adjoint

We briefly discuss quartic terms that can appear in the bi-adjoint Lagrangian. Due to the nature of the bi-adjoint SM gauge charge, there is a large multiplicity of possible bi-adjoint quartic terms. Recalling SU(3) tensor product rules we have [45, 46]

$$8 \otimes 8 = 1 \oplus 8 \oplus 8_s \oplus 10_s \oplus \overline{10}_s \oplus 27 \quad (13)$$

The 10 is a 3 index symmetric object. The 27 has two upper and two lower symmetrized indices.

Similarly, we have the tensor product rule for two adjoints of SU(2)

$$3 \otimes 3 = 1 \oplus 3 \oplus 5 \quad (14)$$

where the 5 of $SU(2)$ is the four index symmetric object.

We see we have 12 possible contractions of the $SU(3)$ and $SU(2)$ indices of 4 bi-adjoint fields. To categorize the different $SU(2)$ and $SU(3)$ contractions we use lower case Roman letters to indicate the fundamental $SU(2)$ indices of the fields. We also indicate fundamental $SU(3)$ indices of bi-adjoint bilinears with Greek letters.

For the real model we can categorize these quartics

$$\begin{aligned}
L \supset & y_1(\phi_{ij}\phi^{ij})(\phi_{lk}\phi^{kl}) + y_2(\phi_i^j\phi_j^k)(\phi_k^l\phi_l^i) + y_3(\phi_{ij}\phi_{kl})(\phi^{ij}\phi^{kl}) + \\
& y_4(\phi_{ij}\phi^{ij})_\alpha^\beta(\phi_{kl}\phi^{kl})_\beta^\alpha + y_5(\phi_i^j\phi_j^k)_\alpha^\beta(\phi_k^l\phi_l^i)_\beta^\alpha + y_6(\phi_{ij}\phi_{kl})_\alpha^\beta(\phi^{ij}\phi^{kl})_\beta^\alpha \\
& y_7(\phi_{ij}\phi^{ij})_{\gamma\delta}^{\alpha\beta}\epsilon_{\alpha\beta\rho}(\phi_{kl}\phi^{kl})_{\alpha\beta}^{\gamma\delta}\epsilon^{\alpha\beta\rho} + y_8(\phi_i^j\phi_j^k)_{\gamma\delta}^{\alpha\beta}\epsilon_{\alpha\beta\rho}(\phi_k^l\phi_l^i)_{\alpha\beta}^{\gamma\delta}\epsilon^{\alpha\beta\rho} + y_9(\phi_{ij}\phi_{kl})_{\gamma\delta}^{\alpha\beta}\epsilon_{\alpha\beta\rho}(\phi^{ij}\phi^{kl})_{\alpha\beta}^{\gamma\delta}\epsilon^{\alpha\beta\rho} \\
& y_{10}(\phi_{ij}\phi^{ij})_{\alpha\beta}^{\gamma\delta}(\phi_{kl}\phi^{kl})_{\gamma\delta}^{\alpha\beta} + y_{11}(\phi_i^j\phi_j^k)_{\alpha\beta}^{\gamma\delta}(\phi_k^l\phi_l^i)_{\gamma\delta}^{\alpha\beta} + y_{12}(\phi_{ij}\phi_{kl})_{\alpha\beta}^{\gamma\delta}(\phi^{ij}\phi^{kl})_{\gamma\delta}^{\alpha\beta} \quad (15)
\end{aligned}$$

The complex representation has more possible quartics and both ϕ and ϕ^\dagger can appear in quartic terms. There are three types of terms plus their hermitian conjugates

$$\phi^4, \phi^2\phi^{\dagger 2}, \phi\phi^{\dagger 3} + h.c. \quad (16)$$

for a total of 36 terms whose group theory structure follows the equation above.

Acknowledgments

This work was partially supported by the OSU Department of Physics

Statement of Human Authenticity

The authors affirm that all text, images, and conceptual creation put forward in this work are entirely human generated, with no input from generative artificial intelligence (AI). The authors do not consent to the use of this work in the training of generative AI models.

* Electronic address: lmc@physics.osu.edu

† Electronic address: schwind.44@osu.edu

- [1] L. M. Carpenter, T. Murphy, and M. J. Smylie, *LEX-EFT: the Light Exotics Effective Field Theory*, *JHEP* **08** (2023) 050, [[arXiv:2302.01344](https://arxiv.org/abs/2302.01344)].
- [2] L. M. Carpenter, K. Schwind, and T. Murphy, *Leptonic signatures of color-sextet scalars. II. Exploiting unique large-ETmiss signals at the LHC*, *Phys. Rev. D* **109** (2024), no. 7 075010, [[arXiv:2312.09273](https://arxiv.org/abs/2312.09273)].
- [3] L. M. Carpenter, T. Murphy, and K. Schwind, *Leptonic signatures of color-sextet scalars*, *Phys. Rev. D* **106** (2022), no. 11 115006, [[arXiv:2209.04456](https://arxiv.org/abs/2209.04456)].
- [4] L. M. Carpenter, T. Murphy, and T. M. P. Tait, *Phenomenological cornucopia of $SU(3)$ exotica*, *Phys. Rev. D* **105** (2022), no. 3 035014, [[arXiv:2110.11359](https://arxiv.org/abs/2110.11359)].
- [5] L. M. Carpenter and K. Schwind, *Unusual portals to new exotics, the W -gluon portal*, [arXiv:2410.08195](https://arxiv.org/abs/2410.08195).
- [6] L. M. Carpenter, M. J. Smylie, J. M. C. Ramirez, C. McDowell, and D. Whiteson, *New physics in triboson event topologies*, *Phys. Rev. D* **105** (2022), no. 7 075027, [[arXiv:2112.00137](https://arxiv.org/abs/2112.00137)].
- [7] E. C. F. S. Fortes, K. S. Babu, and R. N. Mohapatra, *Flavor Physics Constraints on TeV Scale Color Sextet Scalars*, in *6th International Workshop on Charm Physics*, 11, 2013. [arXiv:1311.4101](https://arxiv.org/abs/1311.4101).
- [8] T. Han, I. Lewis, and Z. Liu, *Colored Resonant Signals at the LHC: Largest Rate and Simplest Topology*, *JHEP* **12** (2010) 085, [[arXiv:1010.4309](https://arxiv.org/abs/1010.4309)].
- [9] T. Han, I. M. Lewis, H. Liu, Z. Liu, and X. Wang, *A guide to diagnosing colored resonances at hadron colliders*, *JHEP* **08** (2023) 173, [[arXiv:2306.00079](https://arxiv.org/abs/2306.00079)].
- [10] A. V. Manohar and M. B. Wise, *Flavor changing neutral currents, an extended scalar sector, and the Higgs production rate at the CERN LHC*, *Phys. Rev. D* **74** (2006) 035009, [[hep-ph/0606172](https://arxiv.org/abs/hep-ph/0606172)].
- [11] L. M. Carpenter and R. Colburn, *Searching for Standard Model Adjoint Scalars with Diboson Resonance Signatures*, *J. High Energy Phys.* **12** (2015) 151, [[arXiv:1509.07869](https://arxiv.org/abs/1509.07869)].
- [12] C.-Y. Chen, A. Freitas, T. Han, and K. S. M. Lee, *Heavy Color-Octet Particles at the LHC*, *J. High Energy Phys.* **05** (2015) 135, [[arXiv:1410.8113](https://arxiv.org/abs/1410.8113)].

- [13] M. Gerbush, T. J. Khoo, D. J. Phalen, A. Pierce, and D. Tucker-Smith, *Color-octet scalars at the CERN LHC*, *Phys. Rev. D* **77** (2008) 095003, [[arXiv:0710.3133](https://arxiv.org/abs/0710.3133)].
- [14] T. Plehn and T. M. P. Tait, *Seeking Sgluons*, *J. Phys. G* **36** (2009) 075001, [[arXiv:0810.3919](https://arxiv.org/abs/0810.3919)].
- [15] G. Cacciapaglia, A. Deandrea, T. Flacke, and A. M. Iyer, *Gluon-Photon Signatures for color octet at the LHC (and beyond)*, *J. High Energy Phys.* **05** (2020) 027, [[arXiv:2002.01474](https://arxiv.org/abs/2002.01474)].
- [16] C. T. Preuss and G. Valencia, *Long-lived electroweak-singlet colored scalars*, *Phys. Rev. D* **104** (2021), no. 9 095030, [[arXiv:2109.01261](https://arxiv.org/abs/2109.01261)].
- [17] A. Hayreter and G. Valencia, *Color-octet scalar decays to a gluon and an electroweak gauge boson in the Manohar-Wise model*, *Phys. Rev. D* **102** (2020), no. 11 115033, [[arXiv:1810.04048](https://arxiv.org/abs/1810.04048)].
- [18] L. M. Carpenter and S. Mantry, *Color-Octet, Electroweak-Doublet Scalars and the CDF Dijet Anomaly*, *Phys. Lett. B* **703** (2011) 479–485, [[arXiv:1104.5528](https://arxiv.org/abs/1104.5528)].
- [19] A. Hayreter and G. Valencia, *LHC constraints on color octet scalars*, *Phys. Rev. D* **96** (2017), no. 3 035004, [[arXiv:1703.04164](https://arxiv.org/abs/1703.04164)].
- [20] H. Georgi and M. Machacek, *DOUBLY CHARGED HIGGS BOSONS*, *Nucl. Phys. B* **262** (1985) 463–477.
- [21] M. S. Chanowitz and M. Golden, *Higgs Boson Triplets With $M(W) = M(Z) \cos \theta \omega$* , *Phys. Lett. B* **165** (1985) 105–108.
- [22] J. F. Gunion, R. Vega, and J. Wudka, *Higgs triplets in the standard model*, *Phys. Rev. D* **42** (1990) 1673–1691.
- [23] J. F. Gunion, H. E. Haber, G. L. Kane, and S. Dawson, *The Higgs Hunter’s Guide*, vol. 80. 2000, CRC Press Boca Raton.
- [24] K. Benakli, M. D. Goodsell, and A.-K. Maier, *Generating mu and Bmu in models with Dirac Gauginos*, *Nucl. Phys. B* **851** (2011) 445–461, [[arXiv:1104.2695](https://arxiv.org/abs/1104.2695)].
- [25] L. M. Carpenter and J. Goodman, *New Calculations in Dirac Gaugino Models: Operators, Expansions, and Effects*, *JHEP* **07** (2015) 107, [[arXiv:1501.05653](https://arxiv.org/abs/1501.05653)].
- [26] L. M. Carpenter and M. J. Smylie, *Exploring the phenomenology of weak adjoint scalars in minimal R-symmetric models*, *JHEP* **02** (2022) 102, [[arXiv:2108.02795](https://arxiv.org/abs/2108.02795)].
- [27] R. Boughezal and F. Petriello, *Precise predictions for Higgs production in models with color-octet scalars*, *Nucl. Phys. B Proc. Suppl.* **205-206** (2010) 289–294, [[arXiv:1006.5773](https://arxiv.org/abs/1006.5773)].
- [28] J. Cao, P. Wan, J. M. Yang, and J. Zhu, *The SM extension with color-octet scalars: diphoton enhancement and global fit of LHC Higgs data*, *JHEP* **08** (2013) 009, [[arXiv:1303.2426](https://arxiv.org/abs/1303.2426)].
- [29] N. D. Christensen and C. Duhr, *FeynRules — Feynman rules made easy*, *Comput. Phys. Commun.* **180** (Sep, 2009) 1614–1641.
- [30] A. Alloul, N. D. Christensen, C. Degrande, C. Duhr, and B. Fuks, *FeynRules 2.0 — A complete toolbox for tree-level phenomenology*, *Comput. Phys. Commun.* **185** (Aug, 2014) 2250–2300.
- [31] C. Degrande, C. Duhr, B. Fuks, D. Grellscheid, O. Mattelaer, and T. Reiter, *UFO — The Universal FeynRules Output*, *Comput. Phys. Commun.* **183** (Jun, 2012) 1201–1214, [[arXiv:1108.2040](https://arxiv.org/abs/1108.2040)].
- [32] J. Alwall, R. Frederix, S. Frixione, V. Hirschi, F. Maltoni, O. Mattelaer, H. S. Shao, T. Stelzer, P. Torrielli, and M. Zaro, *The automated computation of tree-level and next-to-leading order differential cross sections, and their matching to parton shower simulations*, *JHEP* **07** (2014) 079, [[arXiv:1405.0301](https://arxiv.org/abs/1405.0301)].
- [33] M. Jacob and G. Wick, *On the general theory of collisions for particles with spin*, *Ann. Phys.* **281** (2000), no. 1 774–799.
- [34] E. Conte, B. Fuks, and G. Serret, *MADANALYSIS 5, a user-friendly framework for collider phenomenology*, *Comput. Phys. Commun.* **184** (Jan, 2013) 222–256.
- [35] T. Sjöstrand, S. Ask, J. R. Christiansen, R. Corke, N. Desai, P. Ilten, S. Mrenna, S. Prestel, C. O. Rasmussen, and P. Z. Skands, *An introduction to pythia 8.2*, *Comput. Phys. Commun.* **191** (Jun, 2015) 159–177.
- [36] J. Y. Araz, B. Fuks, and G. Polykratis, *Simplified fast detector simulation in madanalysis 5*, *The European Physical Journal C* **81** (Apr., 2021).
- [37] M. Cacciari, G. P. Salam, and G. Soyez, *Fastjet user manual: (for version 3.0.2)*, *The European Physical Journal C* **72** (Mar., 2012).
- [38] M. Cacciari, G. P. Salam, and G. Soyez, *The anti-ktjet clustering algorithm*, *Journal of High Energy Physics* **2008** (Apr., 2008) 063–063.
- [39] D. Kim, S. Lee, H. Jung, D. Kim, J. Kim, and J. Song, *A panoramic study of K-factors for 111 processes at the 14 TeV LHC*, *J. Korean Phys. Soc.* **84** (2024), no. 12 914–926, [[arXiv:2402.16276](https://arxiv.org/abs/2402.16276)].
- [40] B. Dumont, *Implementation of a search for supersymmetry in the di-lepton, multi-jet and missing energy channel (20.3 fb-1; 8 TeV; ATLAS-SUSY-2014-10)*, 2021.
- [41] G. Aad et al., *Search for supersymmetry in events containing a same-flavour opposite-sign dilepton pair, jets, and large missing transverse momentum in $\sqrt{s} = 8$ TeV pp collisions with the atlas detector*, *The European Physical Journal C* **75** (July, 2015).
- [42] **ATLAS** Collaboration, G. Aad et al., *Search for squarks and gluinos in final states with one isolated lepton, jets, and missing transverse momentum at $\sqrt{s} = 13$ with the ATLAS detector*, *Eur. Phys. J. C* **81** (2021), no. 7 600, [[arXiv:2101.01629](https://arxiv.org/abs/2101.01629)]. [Erratum: *Eur.Phys.J.C* 81, 956 (2021)].
- [43] L. M. Carpenter, T. Murphy, and M. J. Smylie, *Changing patterns in electroweak precision fits with new color-charged states: Oblique corrections and the W-boson mass*, *Phys. Rev. D* **106** (2022), no. 5 055005, [[arXiv:2204.08546](https://arxiv.org/abs/2204.08546)].
- [44] B. Field, *Distinguishing scalar from pseudoscalar Higgs production at the CERN LHC*, *Phys. Rev. D* **66** (2002) 114007, [[hep-ph/0208262](https://arxiv.org/abs/hep-ph/0208262)].
- [45] S. Coleman, *Fun with SU(3)*, in *Seminar on high-energy physics and elementary particles*, pp. 331–352, 1965, International Atomic Energy Agency Vienna.
- [46] R. Slansky, *Group Theory for Unified Model Building*, *Phys. Rept.* **79** (1981) 1–128.